

Front-back asymmetry controls the impact of viscoelasticity on helical swimming

Veronica Angeles ¹, Francisco A. Godínez ^{2,3}, Jhonny A. Punte-Velazquez ¹,
Rodrigo Mendez-Rojano ¹, Eric Lauga ^{4,*} and Roberto Zenit ^{1,5,†}

¹*Instituto de Investigaciones en Materiales, Universidad Nacional Autónoma de México, Apartado Postal 70-360, México Distrito Federal 04510, México*

²*Instituto de Ingeniería, Universidad Nacional Autónoma de México, Apartado Postal 70-360, México Distrito Federal 04510, México*

³*Polo Universitario de Tecnología Avanzada, Universidad Nacional Autónoma de México, Apodaca 66629, Nuevo Leon, México*

⁴*Department of Applied Mathematics and Theoretical Physics, University of Cambridge, Cambridge CB3 0WA, England, United Kingdom*

⁵*Center for Fluid Mechanics, School of Engineering, Brown University, Providence, Rhode Island 02912, USA*



(Received 2 December 2020; accepted 1 April 2021; published 26 April 2021)

We conduct experiments with force-free magnetically driven rigid helical swimmers in Newtonian and viscoelastic (Boger) fluids. By varying the sizes of the swimmer body and its helical tail, we show that the impact of viscoelasticity strongly depends on the swimmer geometry: it can lead to a significant increase of the swimming speed (up to a factor of 5), a similar decrease (also up to a factor of 5), or it can have approximately no impact. Using an analysis of our data along with theoretical modeling we suggest that the influence of viscoelasticity on helical propulsion is controlled by an asymmetry effect, previously reported for dumbbell swimmers, wherein the front-back size mismatch leads to a non-Newtonian elastic force that can either enhance or hinder locomotion.

DOI: [10.1103/PhysRevFluids.6.043102](https://doi.org/10.1103/PhysRevFluids.6.043102)

I. INTRODUCTION

There are several methods exploited by microorganisms to cope with fluid environments dominated by viscous effects [1]. In particular, the majority of motile bacteria use helical flagellar filaments in order to achieve locomotion [2]. These semirigid filaments can be used either in isolation (monotrichous bacteria) or by cells with several helical filaments (peritrichous bacteria), in which case filaments can bundle together to form a single helical structure. Propulsion of the cell is then enabled by the rotation of a helix in the viscous fluid: since a helix is chiral, a rotation around the helical axis bypasses the constraints of Purcell's scallop theorem [3] leading to a viscous thrust along its axis.

The mechanics of helical swimming is well understood in the case of Newtonian flows [4]. However, many of the fluids in which microorganisms move are not Newtonian, ranging from mucus and complex suspensions to biological tissues. As with most flows in which such fluids are involved, the dynamics of swimming microorganisms are significantly affected by viscoelasticity, the presence of shear-dependent stresses, or both. Numerous studies have been devoted to the subject

*e.lauga@damtp.cam.ac.uk

†zenit@brown.edu

[5–13] with some results which appear to be in contradiction with each other, and thus a number of fundamental issues remain open.

One possible starting point to capture the effect of viscoelasticity is the theoretical study in Ref. [5] which extended the classical Taylor waving sheet result to the case of viscoelastic Oldroyd-like fluids. The swimming speed of the sheet normalized by its Newtonian value, U_{NN}/U_N , was calculated at leading order in the waving amplitude to be a decreasing function of the Deborah number. This parameter, which quantifies the relative importance of viscoelasticity in a given flow, is defined as $De = \tau\omega$ where τ is the fluid relaxation time and ω is the angular frequency of the wave. That model predicted that the swimming speed in a viscoelastic fluid is smaller than its Newtonian equivalent for any value of De . While this result reignited interest in the field, its validity is restricted to the case of small wave amplitude and to the case in which the wave is not affected by the nature of the surrounding fluid (the so-called fixed-kinematics limit). In that limit, both experiments [7] and numerical simulations [11] have shown this prediction to be correct.

In contrast with the result above, numerical computations found that when the amplitude of oscillation was not small the swimming speed in the viscoelastic fluid could be larger than that in the Newtonian fluid [14]. Several experimental studies have subsequently confirmed that a faster speed in viscoelastic media was indeed possible [6,9]. The possibility of obtaining both a decrease and an increase in swimming was reported in Ref. [13] where experimental measurements for the ratio of swimming speeds for three different swimming strategies at fixed De number showed that the swimming ratio could be smaller than, larger than, or close to 1 depending on the swimming kinematics. In other words, the swimming speed in a viscoelastic fluid does not depend solely on the value of the De number. A recent analysis of the effect of the swimming gait on locomotion in non-Newtonian media obtained theoretical predictions in good agreement with experiments so far [15].

Given the complexity that arises from swimming in which the waving shape of the appendages might depend on the flow itself via mechanical feedback, it is simpler to focus first on the case for which the kinematics are fixed. A fundamental biological example where the shape is known to be essentially rigid and unchanged by the fluids is the rotating helical filaments of swimming bacteria. The work in Refs. [16,17] extended the Taylor swimming sheet result from Ref. [5] to the case of a helix in the limiting case of a small pitch angle θ (i.e., the angle between the helix axis and the local tangent along the helix center line). They obtained the same decreasing trend of the normalized swimming speed with Deborah number as in Ref. [5]. Subsequent experiments with force-free helices driven in rotation showed, in contrast, that the helical swimming speed could be larger than that in the Newtonian case [6]. Specifically, the swimming speed was shown to depend on both the value of the Deborah number and the shape of the helix; in particular, helices with larger pitch angles produced a more pronounced increase in swimming. However, only two values of the pitch angles were tested experimentally [6]. Subsequent numerical simulations confirmed that the normalized swimming speed could be smaller or larger than 1, depending on both Deborah number and the geometry of the helix [11].

It is therefore clear that, in addition to the expected dependence on the value of the Deborah number, the geometrical properties of a helix impact its free-swimming speed in non-Newtonian fluid. In this paper, we conduct experiments with force-free magnetically driven rigid helical swimmers in Newtonian and viscoelastic (Boger) fluids. We measure the swimming speeds for helices with many different geometries and head sizes. In agreement with previous studies, we find that depending on the helical geometry their swimming speeds can either increase significantly (up to a factor of 5), decrease (also up to a factor of 5), or remain approximately unchanged. The increasing vs decreasing nature of the normalized swimming speed appears in all our experiments to be correlated with the front-back asymmetry in size of the swimmer: when the helix has a larger diameter than the head, a swimming speed larger than the Newtonian value is observed, and vice versa. The impact of viscoelasticity on helical swimming seems thus to be controlled by an asymmetry effect, previously proposed theoretically [18] and corroborated experimentally [19], wherein an elastic force driven by normal stress differences is induced in the viscoelastic fluid by the

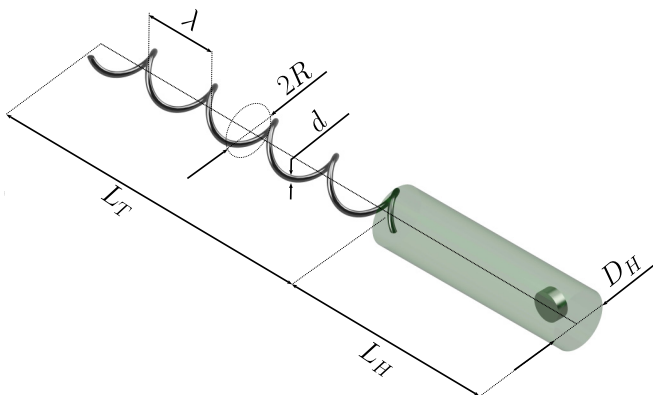


FIG. 1. Sketch of the design parameters of the magnetically driven rigid helical swimmers with a cylindrical head and helical tail. Helix parameters: R is the radius, λ is the wavelength (pitch), L_T is the projected length, d is the diameter of the helical filament. Head: length L_H and diameter D_H .

rotation of the swimmer. Adapting past modeling [18], we show, in agreement with our experiments, that this elastic force can then either hinder or enhance propulsion depending on the ratio between the size of the swimmer's body and that of its helical tail.

The paper is organized as follows. In Sec. II we summarize our experimental setup and parameters. We next present our experimental results in Sec. III. The physical interpretation of our results in light of the asymmetric mechanism is then proposed in Sec. IV.

II. EXPERIMENTAL SETUP

A. Helical swimmers

The experimental design is similar to that previously used in Ref. [20]. Different magnetically actuated force-free swimmers consisting of a tubular plastic head with a rigid helix tail are placed inside a test fluid. By inserting a small permanent magnet inside the head, the swimmers can be made to rotate under the action of an external rotating magnetic field [21]. The shape of the swimmers is depicted schematically in Fig. 1. A right-handed rigid helix is placed at the other end of the cylindrical head. In all cases, both the size of the head (length L_H and diameter D_H) and the helix (contour length L , projected length L_T , radius R , wavelength λ , and filament diameter d) are varied in order to explore the effect of geometry and a total of ten different swimmer geometries are tested. The geometrical parameters are shown in Table I for all swimmers used in this paper. The first five swimmers (F1 and R1 to R4) had tails made of steel wire (Young's modulus $E \approx 207$ GPa). The second set of swimmers (A1 to A5) was three-dimensionally printed with tails fabricated with a polymeric resin. The pitch angle of the helix, θ , defined as $\tan \theta = 2\pi R/\lambda$ varies in our experiments from 29° to 77° .

B. Rotation

The rotation of the head leads to the rotation of the helical tail, which in turn produces the thrust force that propels the swimmer through the fluid. The rotation frequency of the external magnetic field, measured with a digital tachometer, ranged from 0.41 to 5.8 Hz, with a different range for each swimmer. All experiments were conducted below the step-out frequency so that swimmers always rotate with the external frequency.

Note that the swimmers studied here do not capture one important aspect of helically propelled organisms. In our case, the head and the helix swimmer rotate in the same direction. In contrast, in a

TABLE I. Dimensions of the ten helical swimmers used in this paper; all lengths are in millimeters. Here L is the total contour length of the tail, θ is the pitch angle in radians (degrees), and all other symbols are defined in Fig. 1. The empty and solid symbols represent experiments conducted in Newtonian and Boger fluids, respectively.

Swimmer	L_H	D_H	L	d	λ	$2R$	R/λ	θ	$D^* = 2R/D_H$	L_T
F1 ($\triangle, \blacktriangle$)	14.3	4.0	58	0.3	7.6	3.5	0.23	0.97 (55°)	0.88	35.7
R1 (\circ, \bullet)	23	3.0	65	0.9	10.0	1.8	0.09	0.52 (29°)	0.60	56.8
R2 (\square, \blacksquare)	23	3.0	65	0.9	10.0	3.2	0.16	0.79 (45°)	1.07	45.9
R3 ($\nabla, \blacktriangledown$)	23	3.0	65	0.9	10.0	4.6	0.23	0.96 (55°)	1.53	37.3
R4 (\diamond, \blacklozenge)	23	3.0	65	0.9	10.0	11.8	0.59	1.31 (75°)	3.93	16.8
A1 ($\triangleleft, \blacktriangleleft$)	17.3	4.1	76	1.0	9.5	3.0	0.16	0.75 (45°)	0.73	54.3
A2 ($\triangleright, \blacktriangleright$)	17.3	4.1	80	1.0	9.5	7.0	0.37	1.13 (67°)	1.71	39.36
A3 ($\triangle, \blacktriangle$)	17.3	4.1	83	1.0	9.5	15.0	0.79	1.34 (77°)	3.66	23.2
A4 (\circ, \bullet)	17.3	4.1	80	1.0	5.0	3.5	0.35	1.13 (65°)	0.85	37.6
A5 (\square, \blacksquare)	17.3	4.1	80	1.0	13.0	9.0	0.35	1.13 (65°)	2.20	37.2

swimming bacterium, due to the torque-free constraint the helical flagellar filament counter-rotates relative to the cell body [2], a case that is not addressed in our paper.

C. Test fluids

Two types of fluids were used, namely, Newtonian and viscoelastic (Boger). We tested two Newtonian (N1, N2) and two viscoelastic fluids (B1, B2). All fluids were glucose-based: either industrial-grade glucose syrup (series 1) or commercial corn syrup (Karo brand) was used (series 2). While the properties of the industrial-grade syrup varied from batch to batch, commercial corn syrup was found to consistently have the same properties. The viscoelastic fluids (B1, B2) were prepared with glucose, water, and a small amount of polyacrylamide (PAAM), molecular weight 5×10^6 g/mol from Sigma-Aldrich); they were fabricated by slowly dissolving the polyacrylamide in nonionic water for 24 h. Afterwards, the polymeric solution was added to the glucose and the mixture was mixed slowly for four days. We show in Table II the material and rheological properties of the two pairs of test fluids used in this paper. The Newtonian liquids were fabricated by adding water to glucose until the fluid had similar viscosity to that of the viscoelastic fluid, for each case.

TABLE II. Composition and physical properties of the four fluids studied: composition [from glucose (G), water (W), and PAAM], mass density (ρ), dynamic viscosity (μ), power index (n), and mean relaxation time (τ). Note that for N1 and B1 industrial grade glucose syrup was used, while for N2 and B2 commercial corn syrup (Karo brand) was used.

Fluid	G/W/PAAM (%)	ρ kg/m ³	μ Pa s	n	τ s
N1	89/11/0	1390	3.5	1.0	0.0
B1	84.96/15/0.04	1340	3.8	0.98	1.23
N2	89/11/0	1385	1.64	1.0	0.0
B2	84.96/15/0.04	1366	1.64	0.98	1.63

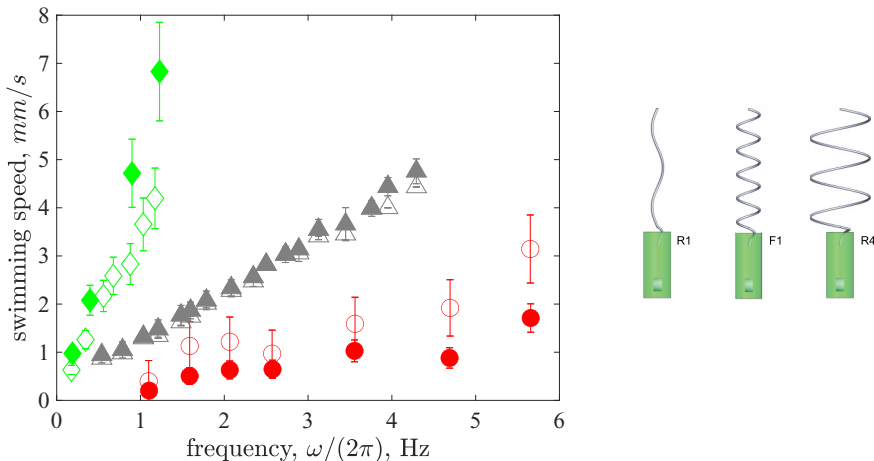


FIG. 2. Measured swimming speed, U , as a function of rotational frequency, $\omega/2\pi$, for three representative swimmers (F1, R1, and R4 from Table I). Empty and filled symbols show the results for Newtonian and viscoelastic fluids, respectively (fluids N1 and B1 from Table II).

The rheological properties of the fluids in Table II were determined using a parallel-plate rheometer with 40-mm diameter and 1-mm gap (TA Instruments, ARES-G2). Both steady and oscillatory tests were conducted to measure the dynamic viscosity, μ , as well as the storage and loss moduli, G' and G'' , respectively. The mean relaxation time τ is calculated by fitting G' and G'' to a generalized Maxwell model [9]. The power index, n , was determined by fitting a power-law model to the steady shear viscosity tests. Finally, the density of the fluids ρ is obtained using a 25-ml pycnometer.

D. Measurements

The motion of the swimmers in both Newtonian and viscoelastic (Boger) fluid was filmed with a digital camera at 60 frames per second. The images were processed digitally with the software Tracker. Each experiment was repeated at least three times to ensure repeatability. The temperature in the experiment ranged between 23 and 24 °C.

III. EXPERIMENTAL RESULTS

Each swimmer was tested in a pair of fluids and its swimming speed was measured as a function of the rotational frequency to compare directly the Newtonian and viscoelastic results. We show in Fig. 2 three selected experimental results illustrating the three possible qualitative results. The swimming speed is plotted as a function of rotational frequency for swimmers F1, R1, and R4 from Table I for the first fluid pair N1 and B1 (see Table II). We see that for a helical swimmer three different behaviors are possible: the swimmer can swim faster in a viscoelastic fluid compared to the Newtonian case (green rhombus), it can go slower (red circles), or it can swim with approximately the same speed (gray triangles). The three swimmers are propelled by the same helical mechanism and the most notable differences between them are their geometrical parameters, specifically the value of their pitch angle, θ , and tail-to-head size ratios, $D^* = 2R/D_H$. The angles range from 29° (slower swimming) to 52° (same speed) to 75° (faster swimming) while the size ratios are $D^* = 0.6$ (slower swimming), 0.88 (same speed), and 3.93 (faster swimming).

To quantify the influence of viscoelasticity on the locomotion, we next calculate the ratio between the swimming speeds, U_{NN}/U_N , where U_{NN} and U_N are the measured mean speeds in the non-Newtonian and Newtonian fluids, respectively. To assess the relative importance of viscoelastic

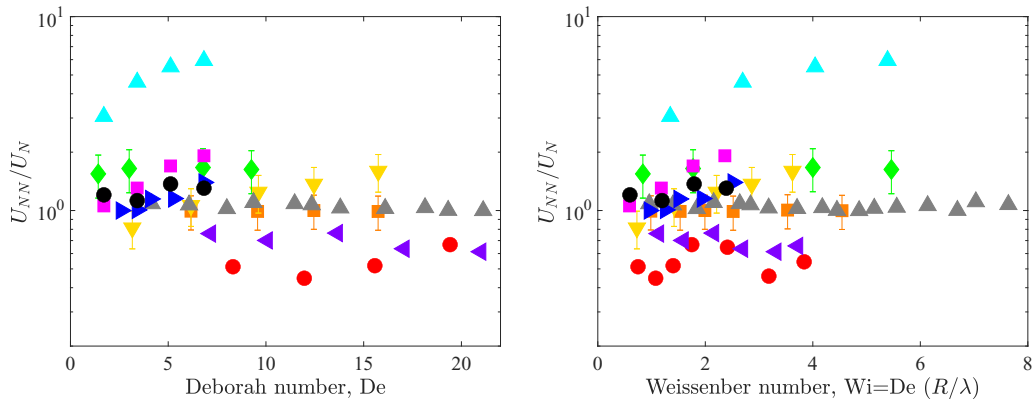


FIG. 3. Ratio of viscoelastic to Newtonian swimming speeds, U_{NN}/U_N , as a function of the Deborah number, De (left), and Weissenberg number, Wi (right). Symbols refer to the swimmers listed in Table I.

effects, we calculate the Deborah number as $De = \omega\tau$, where τ is the fluid relaxation time. The ratio U_{NN}/U_N is then plotted in Fig. 3 (left) as a function of De for all the swimmers from Table I. Despite the large range of Deborah numbers in our experiments (from below 1 to above 20), a clear trend is not apparent in the data.

Instead of the Deborah number, one could argue that the relevant dimensionless parameter to interpret the data is the Weissenberg number, Wi , which, instead of comparing the relaxation time of the fluid with the rotation rate of the swimmer, compares it to the relative rate of deformation in the flow. Hence, we can define this number as $Wi = \dot{\gamma}\tau$, where $\dot{\gamma}$ is the characteristic shear rate. For a rotating helix, the shear rate scales as $R\omega/\lambda$; therefore, we have $Wi \sim (R/\lambda)De$. We plot in Fig. 3 (right) the normalized mean speed U_{NN}/U_N as a function of the Weissenberg number, for all experiments. Similar to the previous case, the data do not show a clear dependence on Wi . These two dimensionless numbers can therefore not be used alone to characterize the changes in swimming speed when viscoelastic effects are present.

Contrasting our data with the experimental results from Ref. [6], we notice that in this work also the dependence of the swimming speeds with De of helices with different pitch angles did not collapse into a single curve. The follow-up numerical study in Ref. [11] showed also that the ratio U_{NN}/U_N was affected by both the Deborah number and the helix pitch angle. Guided by these studies, we replot our data in Fig. 4 (left) with the swimming speed increase now shown as a function of $R/\lambda = \tan\theta/(2\pi)$. Displayed in this manner, we see a remarkably consistent increase of swimming enhancement with R/λ (i.e., with the helix angle, θ) regardless of the value of the Deborah number. A value of $R/\lambda \approx 0.213$, corresponding to a helix angle of $\theta \approx 53.3^\circ$, appears to mark the transition from a decrease to an increase in swimming speed. We have also included the data from Ref. [6] in Fig. 4 (left) (* and \times symbols); the small number of data points in that study appear to fit within the uncertainty of our experiments. Note, however, that the increase in U_{NN}/U_N found by these authors was very modest in comparison to the present data where we obtain increases of up to a factor of 5.

One important aspect of the swimmer geometries shown in Table I is that the size of the head, D_H , remains relatively constant for all swimmers; however, to achieve different pitch angles, the size of the helix, $2R$, varies significantly. Therefore, the helix-to-head size ratio, $D^* = 2R/D_H$, varies from 0.6 to 3.9. The helix diameter can therefore be smaller than, similar to, or larger than the diameter of the head. To explore the way in which this change in geometry affects the swimming speed, we plot in Fig. 4 (right) the normalized swimming speed, U_{NN}/U_N , as a function of the size ratio D^* , for all our experiments. Clearly, and similarly to the results in Fig. 4 (left), a correlation can be identified;

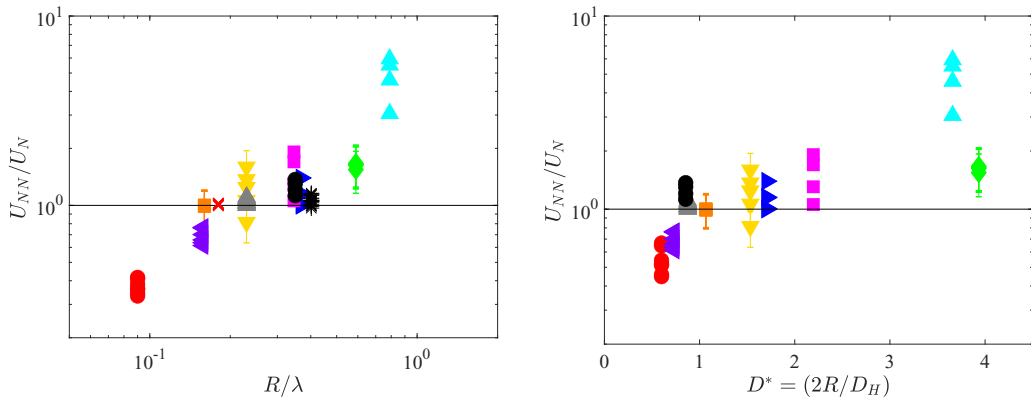


FIG. 4. Left: Ratio of viscoelastic to Newtonian swimming speeds, U_{NN}/U_N , as a function of the helix aspect ratio, R/λ ; the (*) and (x) symbols show the data from Ref. [6] for $R/\lambda = 0.40$ and 0.18 , respectively. Right: Ratio of viscoelastic to Newtonian swimming speeds, U_{NN}/U_N , as a function of helix to head diameter ratio $D^*(= 2R/D_H)$. All filled experimental symbols follow Table I.

when the head is smaller than the helix, the swimming speed in the viscoelastic fluid is larger than the Newtonian one, and when the head is larger then the opposite happens.

IV. PHYSICAL INTERPRETATION

How can we explain theoretically the influence of viscoelasticity on the swimming speed ratio, U_{NN}/U_N ? While viscoelastic effects are undoubtedly important, the values of the Deborah or Weissenberg numbers alone are not able to quantify the impact of elastic stresses on the swimming speed. As shown above, both the helix angle and the helix-to-head size ratio appear to play a role in the balance between thrust and drag on the swimmer. We consider them both separately in what follows.

A. Local resistive model

Using the observation, shown in Fig. 2, that the swimming speed increases approximately linearly with the rotational frequency in all cases, we can first attempt to rationalize the impact of the helical slope using resistive-force theory for low-Reynolds number swimmers [22]. This is known to be valid in the Newtonian case for slender swimmers, and thus should remain approximately valid at small Deborah numbers in the viscoelastic case. The swimming speed of a force-free helix is predicted by the resistive-force theory framework to be given by

$$\left(\frac{U}{\omega R}\right)_N = \frac{(\xi - 1) \tan \theta}{1 + \xi \tan^2 \theta + \xi_0}, \quad (1)$$

where $\xi = c_{\perp}/c_{\parallel}$ is the ratio between the drag coefficient for local portions of the slender helix moving perpendicularly and parallel to the local tangent [22], $\tan \theta$ is the tangent of the helix angle, and $\xi_0 = (L_H c_H \sec \theta)/(L_T c_{\parallel})$ is related to the ratio between the head drag coefficient, c_H , and the parallel helix drag coefficient, c_{\parallel} , and where L_H and L_T are the head and projected tail length, respectively. Assuming the swimmer to only move in the horizontal direction, the value of the resistant coefficient for the cylindrical head is similar to that for the slender body and $c_H \sim c_{\parallel}$. For the swimmers considered here, ξ_0 is then $O(10^{-1})$.

Assuming that a similar local hydrodynamic analysis can be conducted for a viscoelastic Boger fluid at small De , the helix swimming speed would then be given by

$$\left(\frac{U}{\omega R}\right)_{\text{NN}} = \frac{(\xi^{\text{NN}} - 1) \tan \theta}{1 + \xi^{\text{NN}} \tan^2 \theta + \xi_0^{\text{NN}}}, \quad (2)$$

where $\xi^{\text{NN}} = c_{\perp}^{\text{NN}}/c_{\parallel}^{\text{NN}}$ is the drag coefficient ratio and $\xi_0^{\text{NN}} = L_H c_H^{\text{NN}} \sec \theta / (L_T c_{\parallel}^{\text{NN}})$ is the resistance coefficient ratio in a viscoelastic liquid. In contrast to the Newtonian case, ξ_0^{NN} is expected to depend on the value of the translational Weissenberg numbers, $\widehat{\text{Wi}} = \tau U / 2R$ [23]. For the range of speeds tested in the current experiments, $\widehat{\text{Wi}} = O(1)$, for which $c_H^{\text{NN}} \sim c_H$. Therefore, we can expect the value of ξ_0^{NN} to also be small.

Now, assuming that $\xi \approx 2$ in the Newtonian case [22], we obtain

$$\frac{U_{\text{NN}}}{U_N} = (\xi^{\text{NN}} - 1) \left(\frac{1 + 2 \tan^2 \theta + \xi_0}{1 + \xi^{\text{NN}} \tan^2 \theta + \xi_0^{\text{NN}}} \right), \quad (3)$$

which can, theoretically, be smaller or larger than 1 depending on the value of θ , ξ^{NN} , ξ_0 , and ξ_0^{NN} .

Our experimental results from Fig. 4 (left) show that $U_{\text{NN}}/U_N < 1$ for small pitch angles (small R/λ). With small values of ξ_0 and ξ_0^{NN} , Eq. (3) can predict $U_{\text{NN}}/U_N < 1$ for small angles if $1 < \xi^{\text{NN}} < 2$, i.e., for a perpendicular drag that remains larger than the parallel one but less so than in the Newtonian case. In contrast, for large pitch angles (large R/λ), the experiments show that $U_{\text{NN}}/U_N > 1$. With small values of ξ_0 and ξ_0^{NN} , this would be consistent with the model in Eq. (3) only if the drag ratio satisfied $\xi^{\text{NN}} > 2$.

There is therefore a contradiction. Of course, such a local resistive-force theory approach could very well not be valid in a viscoelastic fluid, for example, if nonlocal effects (i.e., hydrodynamic interactions) played an important role. Alternatively, if the local theory was valid, the ratio of drag coefficients ξ^{NN} would have to depend on the value of the angle θ , i.e., the local orientation of the helix relative to the fluid in which it moves. While recent numerical work reported that the elastic stresses in the wake of rigid cylinders depend on the orientation of the cylinder relative to its velocity [24], the dependence of the drag coefficient ratio for different angles in viscoelastic flows has not been reported to date. This resistive-force theory approach does not appear, therefore, to explain the results from Fig. 4 (left) in a physically intuitive way.

B. The asymmetry effect

We can instead provide a physical mechanism for the change in swimming shown in Fig. 4 (right) by turning to past work that addressed the effect of asymmetry for rotating swimmers in viscoelastic fluids. These theoretical [18] and experimental [19] studies showed that a rigid particle in the shape of a snowman, i.e., a dumbbell composed of two spheres of different diameters, would swim in a viscoelastic fluid when rotating about its symmetry axis. The physical origin of the propulsion lies in the secondary flows generated in elastic fluids by normal-stress differences that, for a rotating sphere, lead to fluid flows directed away from the sphere along its rotation axis. A dumbbell made of two spheres of different sizes experiences therefore an imbalance of drag due to these two elastic flows, resulting in swimming. This viscoelastic propulsion force is directed in the direction from the largest to the smallest sphere [18,19].

Our data in Fig. 4 (right) clearly indicate that the front-back asymmetry of the helical swimmers does control the normalized swimming speed. We conjecture therefore that it is the size asymmetry between the head and the tail that leads to an additional viscoelastic force affecting the swimming speed, similarly to the one governing the locomotion of snowman particles. If this mechanism is correct, for locomotion that takes place head-first (the case in our experiments), a swimmer with a head smaller than the helix should swim faster due to this viscoelastic asymmetry effect; conversely, if the head is larger than the tail the swimming speed should decrease. This dependence is indeed what we see in our experiments.

To test this idea quantitatively, we can compare the magnitude of this viscoelastic asymmetry force with the other relevant forces acting on the swimmer. We consider the theoretical expression derived in Ref. [18] to estimate the viscoelastic force resulting from the difference in size between the head and helix. Assuming as a first approximation that this additional viscoelastic force is generated regardless of the detailed shape of the head or helix, and identifying the diameters of the spheres in Ref. [18] with the diameters of the head and helix in our experiment, the asymmetry propulsive force predicted theoretically, P_{asym} , is given by

$$P_{\text{asym}} = c_S \omega \left(\frac{D_H}{2} \right)^2 \text{De} \frac{D^{*3}(D^* - 1)}{(1 + D^*)^5}, \quad (4)$$

where c_S is a viscous drag coefficient ($c_S = k\mu$ where k is a dimensionless shape factor), $D^* = 2R/D_H$ is the size ratio, and $\text{De} = \omega\tau$ is the Deborah number. Next, we assume for simplicity that the helical propulsive force, P_{helix} , and the viscous drag force on the helix, D_{helix} , are similar to those given by the Newtonian resistive-force theory, and so is the drag force on the head of the swimmer, D_{head} . The steady force balance on the swimmer in a viscoelastic fluid is now given by

$$P_{\text{helix}} + P_{\text{asym}} = D_{\text{helix}} + D_{\text{head}}. \quad (5)$$

Using the classical expressions for P_{helix} , D_{helix} , and D_{head} from Ref. [4] and combining them with Eq. (4), the force balance can now be written as

$$\begin{aligned} \omega R(c_{\perp} - c_{\parallel}) \sin \theta L_T + c_S \omega \left(\frac{D_H}{2} \right)^2 \text{De} \frac{D^{*3}(D^* - 1)}{(1 + D^*)^5} \\ = U_{\text{NN}}(c_{\perp} \sin^2 \theta + c_{\parallel} \cos^2 \theta) \frac{L_T}{\cos \theta} + U_{\text{NN}} L_H c_H. \end{aligned} \quad (6)$$

Solving for U_{NN} we can write

$$U_{\text{NN}} = U_N + U_{\text{asym}}, \quad (7)$$

where U_N is the Newtonian swimming velocity given by

$$U_N = \omega R \left(\frac{(\xi - 1) \tan \theta}{1 + \xi \tan^2 \theta + \xi_0} \right), \quad (8)$$

where $L^* = L_H/L_T$ and $\xi_0 = (c_H/c_{\parallel})L^* \sec \theta$ is the normalized head drag coefficient. The additional speed due to asymmetry, U_{asym} , is given by

$$U_{\text{asym}} = \left(\frac{\omega R}{1 + \xi \tan^2 \theta + \xi_0} \right) \times \xi_S \frac{D_H^*}{2 \cos \theta} \text{De} \frac{D^{*2}(D^* - 1)}{(1 + D^*)^5}, \quad (9)$$

with $\xi_S = c_S/c_{\parallel}$ and $D_H^* = D_H/L_T$. Using this model, the additional viscoelastic thrust resulting from the front-back asymmetry leads to the normalized swimming speed written as a sum:

$$\frac{U_{\text{NN}}}{U_N} = 1 + \frac{U_{\text{asym}}}{U_N}, \quad (10)$$

where

$$\frac{U_{\text{asym}}}{U_N} = \frac{\xi_S \text{De}}{2(\xi - 1) \sin \theta} \frac{D_H^*}{D^*} \frac{D^{*2}(D^* - 1)}{(1 + D^*)^5}. \quad (11)$$

This final expression indicates that the viscoelastic contribution due to the asymmetry of the swimmer depends on many factors, including the Deborah number and the size ratio D^* . Importantly, the ratio U_{asym}/U_N can be positive or negative depending on the value of D^* relative to 1. Since $\xi > 1$, swimmers with $D^* > 1$ will swim faster than in the Newtonian fluid while those with $D^* < 1$ will slow down.

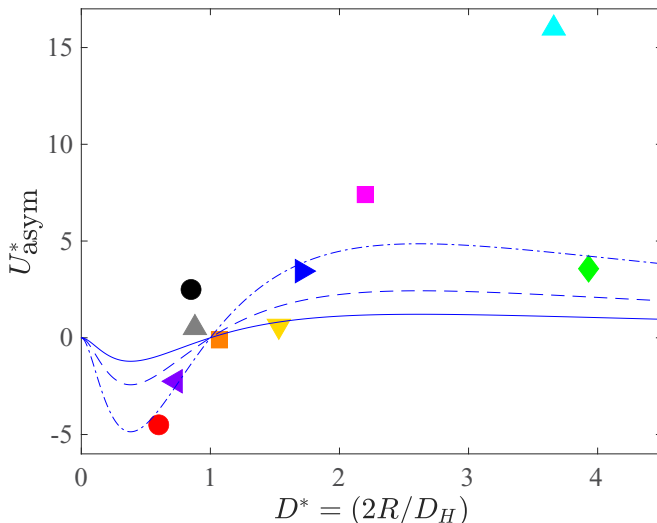


FIG. 5. Modified extra swimming speed, U_{asym}^* , as defined in Eq. (12), as a function of helix to head diameter ratio $D^*(= 2R/D_H)$, for $De \approx 6.8$. The symbols are the experimental values while the lines show the theoretical predictions of the model in Eq. (12) with values $\xi_s = 20$ (solid line), 40 (dashed line), and 80 (dash-dotted line).

To show that Eq. (11) can reproduce the experiment we define U_{asym}^* as

$$U_{\text{asym}}^* = \frac{U_{\text{asym}}}{U_N} \frac{\sin \theta}{D_H^*} = \frac{\xi_s De}{2(\xi - 1)} \frac{D^{*2}(D^* - 1)}{(1 + D^*)^5}. \quad (12)$$

Since both $\sin \theta$ and D_H^* are known quantities in our experiments, the result in Eq. (12) can then be plotted as a function of D^* for given values of De and ξ_s . To do so, we extract data from Fig. 3 (left) for an approximately constant value of $De \approx 6.8$ from which, using Eq. (10), experimental values of U_{asym}^* can be calculated. We show in Fig. 5 the comparison between the model, Eq. (12), and the experimental values using three possible values for the dimensionless factor ξ_s . The model is able to reproduce the experimental trend and shows a clear transition for U_S/U_N from negative to positive values, thus rationalizing the transition from slower to faster than Newtonian when the helix to tail size ratio goes from smaller to larger than unity.

V. CONCLUSION

In summary, we have carried out experiments on the locomotion of free-swimming magnetically driven rigid helices in Newtonian and viscoelastic (Boger) fluids. We varied the sizes of the swimmer's body and its helical tail and showed that the impact of viscoelasticity depends critically on the geometry of the swimmer: it can lead to a large increase of the swimming speed, a decrease, or it can have approximately no impact. We proposed that the influence of viscoelasticity on helical propulsion is controlled by a viscoelastic effect, previously reported for snowmanlike dumbbell swimmers, wherein the front-back asymmetry of the swimmer generates a non-Newtonian elastic propulsion force that can either enhance or hinder locomotion. A simple theoretical model was then formulated to account for this viscoelastic-asymmetry force. It was found that its effect can indeed increase or decrease the swimming speed depending on the head-to-tail size ratio and the Deborah number, in agreement with our experiments.

The obvious next step in this investigation would be to address a similar question for biological swimmers propelled by helical flagellar filaments. The cell body of a swimming bacterium such

as *E. coli* has a width $D_H \approx 0.88 \mu\text{m}$ while the diameters of the helical flagella are $2R \approx 0.4 \mu\text{m}$. The dimensionless ratio, in that case, is therefore given by $D^* = 2R/D_H \approx 0.45$. Since this is less than 1, our results suggest therefore that bacteria self-propelling in similar fluids would have their swimming speed decreased by elastic stresses.

ACKNOWLEDGMENTS

V.A. is grateful to Conacyt-Mexico for a graduate student scholarship and support. This project has received funding from the European Research Council under the European Union's Horizon 2020 research and innovation program (Grant No. 682754 to E.L.).

-
- [1] E. Lauga, *The Fluid Dynamics of Cell Motility* (Cambridge University, Cambridge, England, 2020).
 - [2] E. Lauga, Bacterial hydrodynamics, *Annu. Rev. Fluid Mech.* **48**, 105 (2016).
 - [3] E. M. Purcell, The efficiency of propulsion by rotating flagellum, *Proc. Natl. Acad. Sci. USA* **94**, 11307 (1997).
 - [4] B. Rodenborn, C.-H. Chen, H. L. Swinney, B. Lui, and H. P. Zhang, Propulsion of microorganisms by a helical flagellum, *Proc. Natl. Acad. Sci. USA* **110**, E338 (2013).
 - [5] E. Lauga, Propulsion in a viscoelastic fluid, *Phys. Fluids* **19**, 083104 (2007).
 - [6] B. Liu, T. R. Powers, and K. S. Breuer, Force-free swimming of a model helical flagellum in viscoelastic fluids, *Proc. Natl. Acad. Sci. USA* **108**, 19516 (2011).
 - [7] X. Shen and P. E. Arratia, Undulatory Swimming in Viscoelastic Fluids, *Phys. Rev. Lett.* **106**, 208101 (2011).
 - [8] D. A. Gagnon, X. N. Shen, and P. E. Arratia, Undulatory swimming in fluids with polymer networks, *Europhys. Lett.* **104**, 14004 (2013).
 - [9] J. Espinosa-Garcia, E. Lauga, and R. Zenit, Fluid elasticity increases the locomotion of flexible swimmers, *Phys. Fluids* **25**, 031701 (2013).
 - [10] M. Dasgupta, B. Liu, H. C. Fu, M. Berhanu, K. S. Breuer, T. R. Powers, and A. Kudrolli, Speed of a swimming sheet in Newtonian and viscoelastic fluids, *Phys. Rev. E* **87**, 013015 (2013).
 - [11] S. E. Spagnolie, B. Liu, and T. R. Powers, Locomotion of Helical Bodies in Viscoelastic Fluids: Enhanced Swimming at Large Helical Amplitudes, *Phys. Rev. Lett.* **111**, 068101 (2013).
 - [12] B. Thomases and R. D. Guy, Mechanisms of Elastic Enhancement and Hindrance for Finite-Length Undulatory Swimmers in Viscoelastic Fluids, *Phys. Rev. Lett.* **113**, 098102 (2014).
 - [13] F. A. Godínez, L. Koens, T. D. Montenegro-Johnson, R. Zenit, and E. Lauga, Complex fluids affect low-Reynolds number locomotion in a kinematic-dependent manner, *Exp. Fluids* **56**, 97 (2015).
 - [14] J. Teran, L. Fauci, and M. Shelley, Viscoelastic Fluid Response Can Increase the Speed and Efficiency of a Free Swimmer, *Phys. Rev. Lett.* **104**, 038101 (2010).
 - [15] G. J. Elfring and G. Goyal, The effect of gait on swimming in viscoelastic fluids, *J. Non-Newtonian Fluid Mech.* **234**, 8 (2016).
 - [16] H. C. Fu, T. R. Powers, and C. W. Wolgemuth, Theory of Swimming Filaments in Viscoelastic Media, *Phys. Rev. Lett.* **99**, 258101 (2007).
 - [17] H. C. Fu, C. W. Wolgemuth, and T. R. Powers, Swimming speeds of filaments in nonlinearly viscoelastic fluids, *Phys. Fluids* **21**, 033102 (2009).
 - [18] O. S. Pak, L. Zhu, L. Brandt, and E. Lauga, Micropropulsion and microrheology in complex fluids via symmetry breaking, *Phys. Fluids* **24**, 103102 (2012).
 - [19] J. A. Puente-Velázquez, F. A. Godínez, E. Lauga, and R. Zenit, Viscoelastic propulsion of a rotating dumbbell, *Microfluid. Nanofluid.* **23**, 108 (2019).
 - [20] S. Gomez, F. Godínez, E. Lauga, and R. Zenit, Helical propulsion in shear-thinning fluids, *J. Fluid Mech.* **812**, R3 (2016).
 - [21] F. A. Godínez, O. Chávez, and R. Zenit, Note: Design of a novel rotating magnetic field device, *Rev. Sci. Instrum.* **83**, 066109 (2012).

- [22] C. Brennen and H. Winet, Fluid mechanics of propulsion by cilia and flagella, [Ann. Rev. Fluid. Mech. **9**, 339 \(1977\)](#).
- [23] A. J. Mendoza-Fuentes, O. Manero, and R. Zenit, Evaluation of drag correction factor for spheres settling in associative polymers, [Rheol. Acta **49**, 979 \(2010\)](#).
- [24] C. Li, B. Thomases, and R. D. Guy, Orientation dependent elastic stress concentration at tips of slender objects translating in viscoelastic fluids, [Phys. Rev. Fluids **4**, 031301\(R\) \(2019\)](#).